Int. J. Electrochem. Sci., 9 **(2014)** 6781 - 6792

International Journal of
ELECTROCHEMICAL
SCIENCE
www.electrochemsci.org

Comparative Study on Rate of Flow Accelerated Corrosion (FAC) of API 5L X-52-65-70 Steels in a Brine added with H_2S at 60°C by Using a Rotating Cylinder Electrode (RCE)

A. Cervantes Tobón[1,*], *M. Díaz Cruz*[1], *J. L. González Velázquez*[1], *J. G. Godínez Salcedo*[1], *R. Macías Salinas*[2]

[1]Instituto Politécnico Nacional, Departamento de Ingeniería Metalúrgica, IPN-ESIQIE, U.P. Adolfo López Mateos, Zacatenco, 07738 México, D.F., México.
[2]Instituto Politécnico Nacional, Departamento de Ingeniería Química, UPALM, Col. Zacatenco, Del. G. A. Madero, 07738, México, D.F.
[*]E-mail: maenc_2000@yahoo.com.mx

Received: 15 August 2014 / *Accepted:* 19 September 2014 / *Published:* 29 September 2014

This work focuses on how important the hydrodynamic conditions are on the corrosion rates occurring in steel type API 5L grades such as X52, X65 and X70 when are exposed to synthetic brines with and without H_2S at 60°C. Experiments were conducted using a rotating cylindrical electrode (RCE) under hydrodynamic flow conditions over a rotation range from 0 to 6500 rpm (3.744 m/s). It was found out that the rotation rate affects the electrochemical process that takes place on the steel surface since it increases the corrosion rate when the rotational rate is increased. The effect of H_2S presence on the steel caused substantial corrosion rates as a function of flow rate. Under the presence of H_2S, the corrosion products were composed mainly of iron oxides, one sulphate (mikasaite) and some sulfur as the mackinawite, which was non-adherent and breaks out easily. The steel API 5L X-70 exhibited the best performance under the presence of H_2S at 60°C with respect to the corrosion rate by yielding the lower corrosion values.

Keywords: Corrosion, polarization resistance, rotating cylinder electrode, pipeline steel.

1. INTRODUCTION

Corrosion in aqueous hydrogen sulfide (H_2S) containing environments is a result of an electrochemical reaction (see equation 4), between the metal (Fe) and the corrosive medium (H_2S). The anodic iron reaction (equation 1) and the cathodic hydrogen sulfide reactions (equation 2 and 3) contribute to the net H_2S reaction. In the net H_2S reaction, FeS scales are formed and atomic hydrogen is produced on the steel surface. The FeS scales formed by the hydrogen sulfide may or may not be protective, depending on conditions such as pH, temperature and H_2S partial pressure. H_2S accelerates

the corrosion reaction and for low alloy steels the corrosion rate increase with decreasing pH of the acidic H_2S containing environment [1-5].

Anodic reaction:

$$Fe \rightarrow Fe^{2+} + 2e^{-} \quad (1)$$

Cathodic reactions:

$$H_2S + H_2O \rightarrow H^{+} + HS^{-} + H_2O \quad (2)$$

$$HS^{-} + H_2O \rightarrow H^{+} + S^{2-} + H_2O \quad (3)$$

Net reaction:

$$Fe + H_2S \rightarrow FeS + 2H \quad (4)$$

The H_2S corrosion is affected by both the generation of hydrogen and the diffusion of hydrogen into the steel. Therefore, the role of H_2S is considered to be two-fold; it increases the rate corrosion of steel in aqueous solutions and it prevents the hydrogen recombination reaction. In H_2S containing environments, the absorption of atomic hydrogen into the metal is enhanced by the effect of sulfur containing species to prevent hydrogen recombination. The main corrosion product formed on the surface of steel in H_2S is the ferrous sulfide (FeS), known as mackinawite [6]; however, depending on pH, partial pressure and the oxidation potential of the medium, the sulfides can take different molecular forms (eg FeS_2 or Fe_7S_8) [7].

Most of the corrosion studies of steel in H_2S have been carried out under static conditions, but in pipeline service, the corrosion occurs mainly under active flow conditions [8]. As the transfer of momentum is intensified, the rate at which chemical reactants or reaction products are transported to and from the metal surface is increased, thus increasing the corrosion rate. The rotating cylindrical electrode (RCE) is a tool that allows to perform tests under variable flow conditions at laboratory scale that simulate a stream of corrosive fluid passing on a corroding surface [9-12]. The RCE has many advantages including: small quantities of test solution are required to perform the test [13]. The equipment is simple and of easy to operation, the test is inexpensive in comparation to other tests. Several investigators have used the RCE in order to determinate the influence of turbulent flow conditions on the corrosion rate [9, 14-17].

The present work aims at investigating the effect of the composition, morphology, and protective characteristics of the corrosion products on the deterioration behavior of API 5L-X52-65-70 pipeline steels in brine with kerosene and H_2S by means of rotating cylindrical electrode (RCE), Scanning Electron Microscopy (SEM), X-ray diffraction (XRD) and Electrochemical technique (Potentiodynamic Polarization Resistance).

2. EXPERIMENTAL PROCEDURE

2.1. Test Environment.

The test solution was a brine prepared according to NACE standard 1D-196 [18] with 106.5789 g/l NaCl, 4.4773 g/l $CaCl_2$ $2H_2O$, 2.061 g/l $MgCl_2$ $6H_2O$ and 10% kerosene, 1387.2 ppm of hydrogen sulfide (H_2S) was added. The pH was 3.89 and the temperature of the solution was 60ºC. The test

solution was deaerated with nitrogen gas for a period of 30 minutes as stated in the ASTM G59-97 (Reapproved 2003) [19], to remove dissolved oxygen.

2.2. Experimental set up.

A double bottom cell made of Pyrex glass heated with hot water was used. Cylindrical tests specimens were cut off from actual pipes of 11 mm or more of thickness in the longitudinal direction. The total area exposed of the working electrode was 3.5 cm^2 for both static and dynamic tests. The reference electrode was saturated calomel electrode, and two auxiliary electrodes of sintered graphite rods were used. Before each experiment, the working electrode was polished with grade 600 silicon carbide paper, cleaned with deionized water and degreased with acetone. All electrochemical tests were performed on recently clean prepared samples and fresh solutions.

2.3. Hydrodynamic conditions.

The hydrodynamic simulations of flow velocity in the laboratory were carried out in a RCE made by Radiometer Analytical, type EDI 10000 connected to a Potentiostat/Galvanostat. The corrosion rate of the system was evaluated at different electrode rotation rates. The working electrode rotational speeds used in this study were varied from 0 to 6500 rpm (3.744 m/s), with increments of 500 rpm. The selection of these ranges were based on the conditions commonly observed at industrial facilities, as well as on the values of the Reynolds numbers (Re) allowing the validation of the existent hydrodynamic and mass transfer correlations for the RCE.

2.4. Corrosion rate measurements.

For Conducting Potentiodynamic Polarization Resistance Measurements a "Standard Test Method for Conducting Potentiodynamic Polarization Resistance Measurements"[19] (ASTM G59-97 (Reapproved 2003)) was applied by means of the commercial software POWER SUIT of Princeton Applied Research by using a Potentiostat/Galvanostat Princeton Applied Research model 263A (over the range of ± 20 mV). The polarization curves were obtained at a rate of 0.166 mV per second. The corrosion rate was obtained as a function of flow rate for the steels used in brine added with 10% of kerosene containing H_2S at 60°C. To ensure the reliable results three readings were taken for each flow velocity range employed, allowing the system to stabilize for 5 minutes before running the test and retake the reading of both the potential and the corrosion rate for each of the steel used in the investigation.

2.5. Characterization of corrosion products by SEM.

The surface morphology and composition of the corrosion products formed on electrode surface was characterized and analyzed using a JEOL 6300 SEM coupled with EDX.

2.5.1 Physical characterization by XRD

X-ray diffraction (XRD) was used to determine the iron phases on API 5L-X52 and X70 steels, with a scanned range from 20° to 90° and a step width of 0.02°, using a Panalytical model XPert MRD diffractometer with Cu Kα radiation. Further, analyses of XRD spectra were carried out using the CreaFit 2.2 DRXWin program.

3. RESULTS AND DISCUSSION

3.1. Chemical analysis and metallographic.

The chemical compositions (wt.%) of the steels employed in the present study were determinate means analysis by optical emission with a bow and spark spectrometer (BELEC), results are shown in Table 1.

Table 1. Chemical composition of the API 5L X-52 and X-65 steels (wt.%).

Steel	C	Mn	Si	P	S	Cr	Cu	Ni	Fe
API 5L X-52	0.111	0.955	0.175	0.005	0.022	0.037	0.293	0.013	98.3
API 5L X-65	0.154	1.357	0.231	0.023	0.014	0.061	0.001	0.022	98.0
API 5L X-70	0.240	1.081	0.284	0.019	0.021	0.156	0.185	0.088	97.8

3.2 Microestructure and grain size

Table 2. Quantification of phases for steels used in the present investigation along the longitudinal section.

Steel	% Ferrite	% Pearlite	ASTM Grain
API 5L X-52	86.64	13.35	8
API 5L X-65	80.57	19.42	9
API 5L X-70	70.51	29.48	10

The microstructure of the steels is shown in Figure 1 depicting pearlite colonies distributed over a ferrite matrix; this is in agreement with similar microestructure obtained by others [20-22].

Table 2 shows the contents of ferrite, pearlite and grain size of the samples with the same magnification:

For API 5L X-52 the percentage of pearlite according to Table 2 is 13.35% and 86.64% ferrite, in the case of API 5L X-65 is 19.42% and 80.57% ferrite and API 5L X-70 has 29.48% pearlite and 70.51% of ferrite. With respect to the grain size (Table 2), the API 5L X-52 has a value of 8 and this is a larger grain with respect to the API 5L X65 obtaining a value of 9 and for the API 5L X-70 according to ASTM.

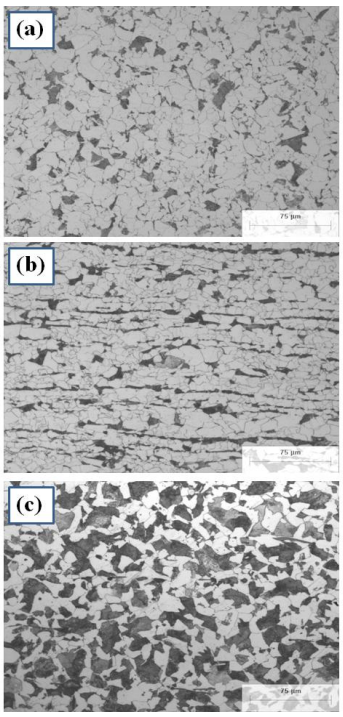

Figure 1. Microstructure of (a) API 5L X-52, (b) API 5L X-65 and (c) API 5L X-70 steels.

3.3 Linear polarization studies

3.3.1 Comparison of the corrosion potentials as function of flow rates for steels API 5L X-52, API 5L X-65 and API 5L X-70 in brine NACE 1D-196 with H_2S at 60°C.

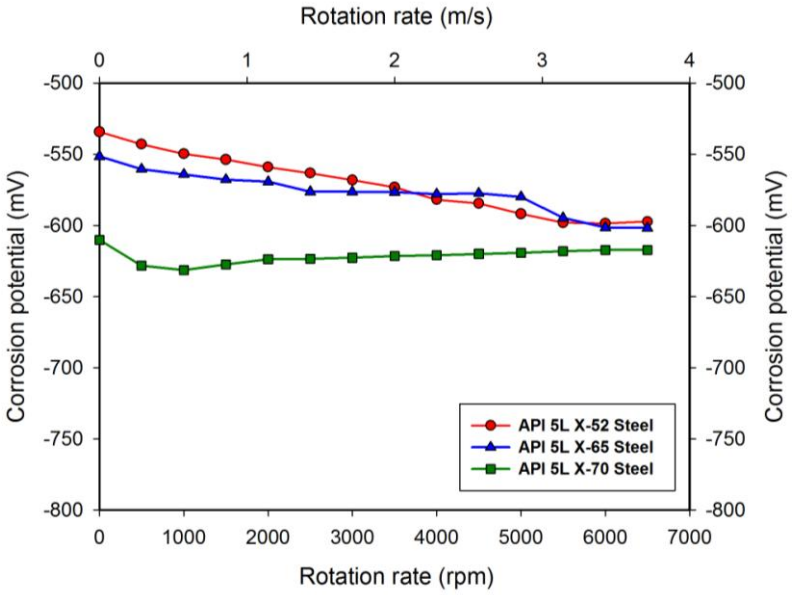

Figure 2. Corrosion potential (corrosion tendency) as a function of the flow rate for API 5L X-52, API 5L X-65 and API 5L X-70 steel in brine added with kerosene in presence of H_2S at 60°C.

Figure 2 shows the results of the corrosion potential (corrosion tendency) of the studied steels as a function of flow rate at 60°C in brine added with kerosene and H_2S. These results shows that the corrosion tendency is greater for the API 5L X-70; in this case the highest activity indicates corrosion products begin to form and evolve uniformly throughout the flow velocity range employed, therefore it is not further seen a significant increase in the tendency to corrosion due to the corrosion potential does not increased greatly, so it could be assumed that the corrosion products formed are more stable and uniform surface API 5L X-70.

In the case of API 5L X-52 and API 5L X-65, both start with a less active corrosion potential and is increased continuously which it may indicate a steady growth of corrosion products which it would in turn indicate that likely there is also a greater amount of those on the surface of the steel. In all cases the corrosion potential became more positive for the API 5L X-52 is from -534.363 to -597.438 mV_{SCE}, API 5L X-65 is from -551.6203 to -601.8060 mV_{SCE} and for the API 5L X-70 is from -610.305 to -617.435 mV_{SCE}. In general, there are two causes of a positive shift of the corrosion potential; either the cathodic process on metal surface is promoted, or the anodic process is restrained [23].

3.3.2 Comparison of the corrosion rates as function of flow rates for steels API 5L X-52, API 5L X-65 and API 5L X-70 in brine NACE 1D-196 with H_2S at 60°C.

As showing in Figure 3 the results for the rate of corrosion of steel API 5L X-52, API 5L X-65 and API 5L X-70 in a medium added with brine kerosene and H_2S at 60°C, are compared to confirm which has the best behavior with respect to corrosion. From these results, it was observed that for all steels from the beginning corrosion rate is increased as increasing flow rate (this variation by the dependence of the corrosion rate on the flow velocity is generally attributed to a change by the corrosion mechanism [24]).

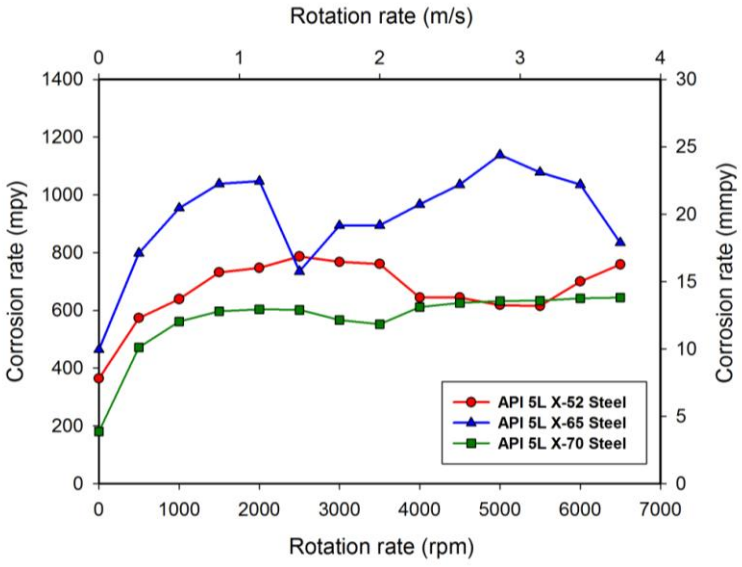

Figure 3. Corrosion rate comparison as a function of the flow rate for the API 5L X-52, API 5L X-65 and API 5L X-70 steel in brine added with kerosene in presence of H_2S at 60°C.

Up to a rotation speed of 3500 rpm, from there (4000 rpm) API 5L X-52 and X-70 steels show similar behavior to maintain a corrosion rate almost constant up to 5,500 rpm, and is the API 5L X-70 which maintains this behavior to the end of the test (6500 rpm), thus suggesting that the corrosion products formed on the surface are more stable (there is not detachment from the corrosion products) and makes the corrosion rate remains almost constant in this range. The API 5L X-52 between 6000 and 6500 rpm shows an increase in the corrosion rate which indicates that there was a detachment of corrosion products formed due to the same action of the flow (inducing movement to the fluid, the wall shear stresses diminish the thickness of this layer [25], which lead to an increase of the corrosion rate), so these may not be as stable or have a good adherence as compared to the other steel. For the case of the API 5L X-65, it has the greater values or corrosion rate compared to the others steels, at 2500 rpm it observed a decrease due the formation of corrosion products and from 3000 rpm the corrosion rate is increased may lead to the detachment of the corrosion products from the surface, but at 5000 to 6500 rpm the corrosion rate decreases again due the continuous formation of corrosion products in the surface of this steel, but the corrosion rate its larger compared with the others steels.

From the above, it was observed that the API 5L X-70 has a better performance in terms of corrosion rate; the better performance attributed to its more uniform formation of corrosion products (oxides, sulfides and one sulfate) and also according to their chemical composition (Table 2) has a higher content of chromium and nickel whose elements that together significantly yield further decrease of the corrosion rate as suggested by Y.S. Choi et al [26].

3.4 SEM surface characterization

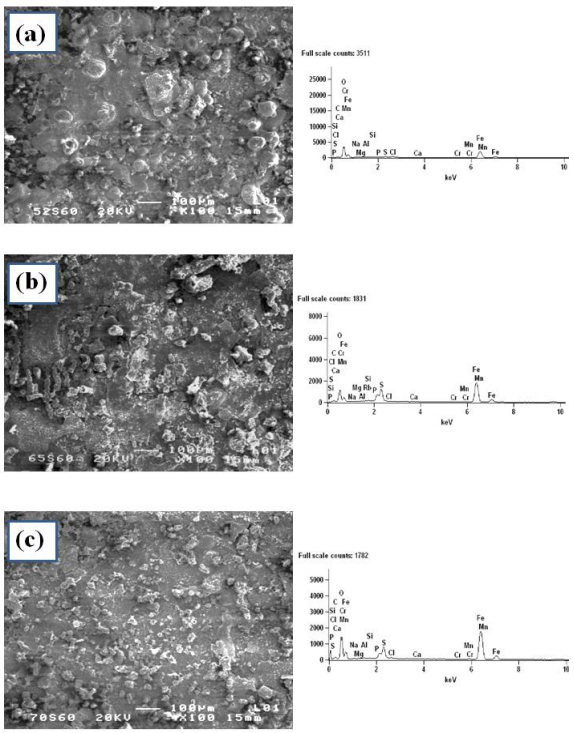

Figure 4. SEM micrographs and EDX microanalysis obtained for (a) API 5L X-52, (b) API 5L X-65 and (c) API 5L X-70 steel surface.

Corrosive deposits from steel formed in solution are mainly composed of insoluble products, undissolved constituents and trace amounts of alloying elements. They formed various oxides and sulfides as a result of the corrosion process undergone by the metal under certain conditions or the type of medium used.

Figures 4 (a), (b) and (c) are SEM micrographs of the corrosion products formed on surfaces of the steels API 5L X-52, API 5L X-65 and X-70 at 100X magnification. In all cases a layer of amorphous corrosion products on the surface generalized being most visibly abundant and porous for API 5L X-52 and API 5L X-65.

3.4.1 EDS Surface characterization

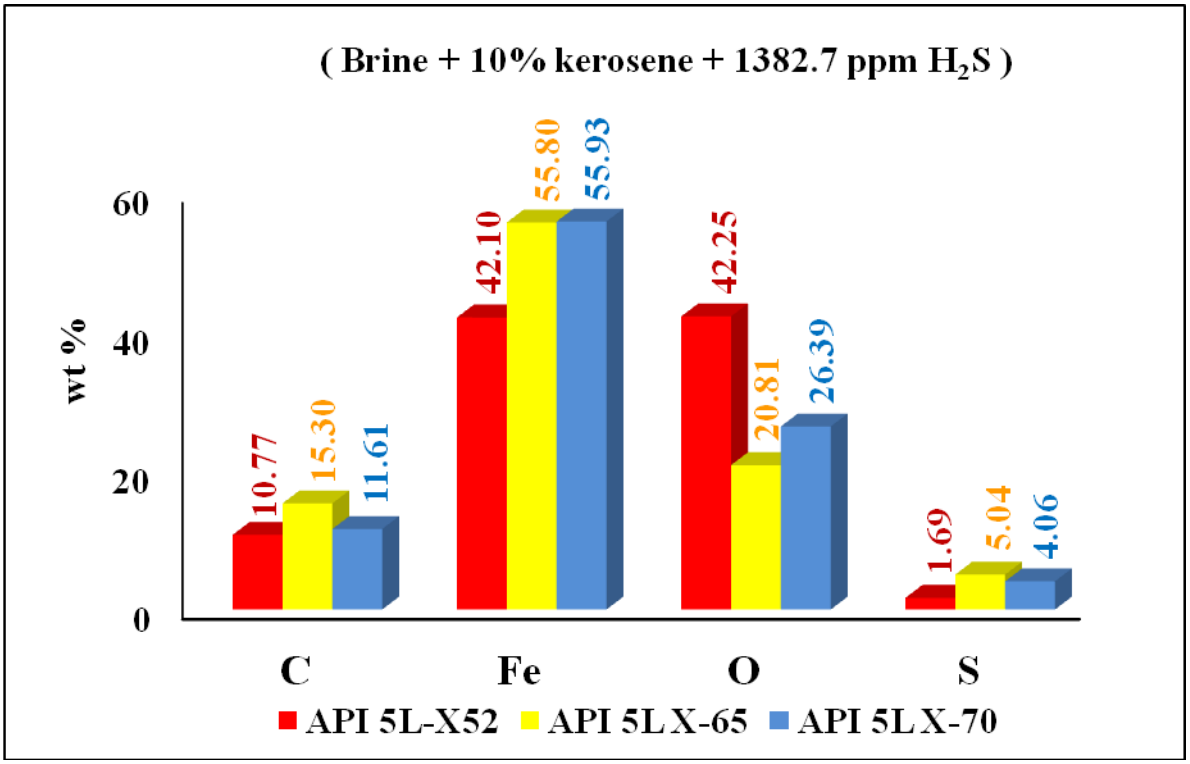

Figure 5. Chemical composition (wt%) of corrosion scale on API 5L X-52, API 5L X-65 and API 5L X-70 steel surface.

Figure 5 EDS depicts the measurements of (a) API 5L X-52, (b) API 5L X-65 and (c) API 5L X-70 steel surfaces (from figure 4) in brine added with kerosene and H_2S at 60°C primarily showing that the mainly identified elements are C, O, Fe. These elements on the surface indicating the presence of the protective FeO, Fe_2O_3, Fe_3O_4 or some sulfides as mackinawite (FeS_{1-x}),film formation (corrosion products) as reported in the literature [27-29]. It is known that H_2S contributes to the corrosion and formation of iron sulfide film. This film is formed almost instantaneously at the moment that the H_2S is added into the solution (brine) and has a black color; mackinawite is the first corrosion product formed at the iron/steel surface and usually forms as a precursor to other types of sulfides. The

mackinawite film formed at the steel surface is nonadherent and cracks easily as report Shoesmith et al [30].

Figure 5 shows too that for the API 5L X-52 corrosion products consist of a 42.10 wt% iron, 42.10% oxygen and 1.69 wt% sulfur, so it is a mixture of oxides with sulfides, for the API 5L X-65 has 55.80 wt% iron, 20.81 wt% oxygen and 5.04 wt% sulfur and for API 5L X-70 has a 55.93% wt of iron, 26.39 wt% oxygen and 4.06 wt% sulfur, which be observed a mixture of oxides with sulfides, but in the cases of API 5L X-65 and X-70 there will be more sulfides than oxides. In API 5L X-52 predominate over sulfide oxides for having a stronger presence of oxygen. For API 5L X-52, although it forms a greater quantity of corrosion products are mostly oxides (less sulfides) which appear to be less adherent and suffer some detachment by the action of flow to rise the corrosion rate again, accordingly.

3.4.2 XRD Characterization of corrosion products

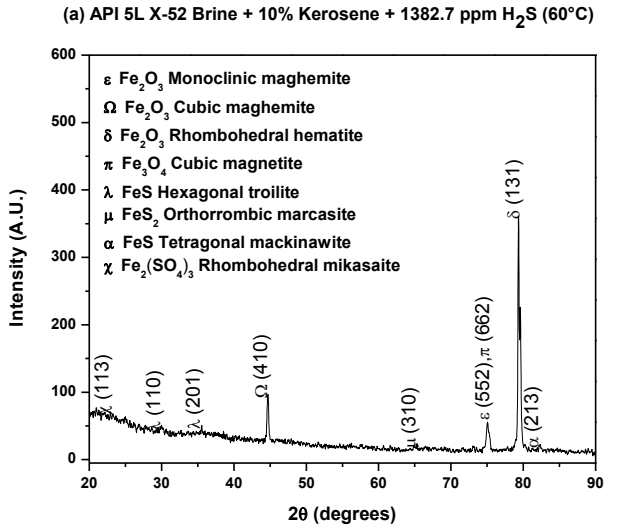

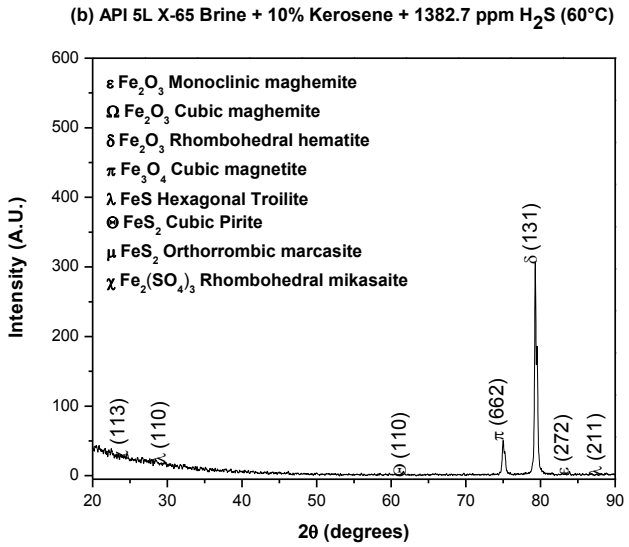

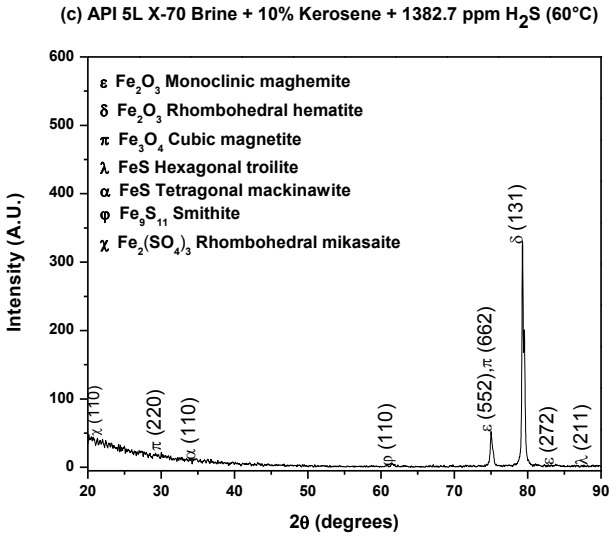

Figure 6. X-ray diffraction analysis (XRD) of corrosion products in (a) API 5L X-52, (b) API 5L X-65 and (c) API 5L X-70 steel surface in brine added with kerosene and H_2S at 60°C.

The study by X-ray diffraction of the corrosion products formed is revealed by Figure 6 for the steels API 5L X-52, X-65 and X-70 consisted with a mixture of oxides and sulfurs as similar as those reported by Hernández et al [31], but also in this case sulfate additionally is formed known as mikasaite ($Fe_2(SO_4)_3$ rhombohedral), which certainly influences the behavior of the corrosion rate and should be studied in more detail to know for sure that the effect on the corrosion rate. The dissolved Fe^{2+} from the substrate (steel) formed iron oxides and the sulfate in this case the rhombohedral mikasaite. Sun Ah Park et al [32] report recently the presence of this compound, in this work the $Fe_2(SO_4)_3$ is a protective layer on carbon steel surfaces.

The three steels are mainly formed oxides hematite (rhombohedral), maghemite (monoclinic and cubic) and magnetite (cubic) and besides sulphides mackinawite (tetragonal) form sulfides other species as are troilite (hexagonal), the smithite and marcasite (orthorrombic). Mackinawite is a common mineral composed of tetragonal crystals, whereas troilite is hexagonal and both are consider protective layers. The different crystal structures of iron sulfides formed in H_2S containing corrosive media were described in detail by Rickard et al [33]. The crystal structures or the corrosion product film significantly vary from each other [34]. The differences of the crystal structures of iron sulfide are due to the corrosive medium differences [35]. The presence of some oxides as Fe_2O_3 and Fe_3O_4 [36], partially protects the steel surfaces from further dissolutions and leads in turn to the appearance of a passive region on the behavior of the corrosion rate as seen in some region of the graph the figure 3 (4000 to 5000 rpm) for the API 5L X-52 and API 5L X-70 steels. The intensity of the peaks detected in the case of API 5L X-52 are more intense which indicates that there is a higher amount of the corrosion products formed on the surface. Therefore in all steels corrosion products are acting as a protective film against the corrosion process being in the API 5L X-70 are more homogeneous, stable for having more sulfides than oxides, therefore be reflected in the better behavior of the three steels used in the investigation with respect to the corrosion rate.

4. CONCLUSIONS

Characterization studies carried out by SEM showed that the corrosion products formed on the surface of each of the steels are composed of a mixture of oxides, sulfides and a sulfate.

The API 5L X-70 steel showed the best behavior with respect to the corrosion rate since it has a lower corrosion rate compared to API 5L X-52 and API 5L X-65; steel, in this case, the flow rate does not have any significant effect on the formation of corrosion products, due to its corrosion products are more stable and uniform in surface although are at a lower amount as could it be seen, the greater presence of sulfides (hexagonal troilite, tetragonal mackinawite and smithite) and one sulfate (rhombohedral mikasaite) helps the improved protection work as oxides (monoclinic and cubic maghemite, rhombohedral hematite and cubic magnetite) protective modifying properties as observed in the API 5L-X52 steel where there is an increased presence of these and serve as a partially protective barrier but are not as efficient as in the case of the API 5L X-70 steel. The best performance that has the API 5L-X70 steel with respect to the corrosion rate is also due to the presence of a greater amount of chromium and nickel which together help to improve the performance with respect to corrosion as suggested by some authors. The present study provides a comparative study of three steels regarding the corrosion rate and the effect of corrosion products that form on the surface.

ACKNOWLEDGEMENTS
The authors would like to thank the Consejo Nacional de Ciencia y Tecnología (CONACYT), Instituto Politécnico Nacional (IPN) for the grant awarded to Mr. Cervantes-Tobón, requerided to develop this work and the Group of Ducts Integrity Analysis (GAID) the sponsorship of this research.

References

1. R. D. Kane and M.S. Cayard, CORROSION 98, 1998.
2. H. Huang and W. Shaw, Corros. Sci., 34 (1) (1993) 61-78.
3. B. Beidokhti, A. Dolati, and A. Koukabi, Materials Science and Engineering: A, 507 (1) (2009) 167-173.
4. O.I. Radkevych and V.I. Pokhmurs'kyi, Materials Sci., 37 (2) (2001) 319-332.
5. R.D. Kane, International Metals Review, 30 (1) (1985) 291-301.
6. F. H. Meyer, O. L. Riggs, R. L. McGlasson, J. D. Sudbury, *Corrosion*, 14 (1958) 69.
7. G. Schmitt, W. Bruckhoff, CORROSION, 620, NACE International, Houston, 1989.
8. T.Y. Chen, A. A. Moccari, D. D. Macdonald, *Corros.*, 48 (1992) 239.
9. D.C. Silverman, *Corros*., 40 (1984) 220.
10. D.C. Silverman, *Corros*., 55 (1999) 1115.
11. R.A. Holser, G. Prentice, R.B. Pond, R. J. Guanti, *Corros*., 48 (1992).
12. L. Shreir, in: Corrosion 1, Metal/Enviroment Reactions (Eds. L.L. Shreir, R. A.. Jarman, G.T. Burstein), 3th Edition, Butterwoths, london 1994, 2:12-2:13.
13. ASTM G 170-01, "Evaluating and Qualifying Oilfield and Refinery Corrosion Inhibitors in the Laboratory", ASTM International (1996) 6-8.
14. D.C. Silverman, *J. Electrochem. Soc*., 44 (1988) 42.
15. S. Nesic, J. Bienkowski, K. Bremhorst, K.S. Yang, *Corros.*, 56 (2000) 1005.
16. K.D. Efird, E.J. Wright, J.A. Boros, T.g. Halley, *Corros*., 49 (1993) 992.
17. B. Poulson, *Corros. Sci*., 23 (1983) 391.

18. NACE 1D-196: "Laboratory Test Methods for Evaluating Oilfield Corrosion Inhibitors" (Houston TX: NACE, 1996).
19. ASTM G59-97 (Reapproved 2003) "Standard Test Method for Conducting Potentiodynamic Polarization Resistance Measurements" (Houston TX: NACE, 2003).
20. R. Dong, I. Sun, Z. Liu, X. Wang and Q. Liu, *Journal of Iron and Steel Research International*, 15 (2008) 71.
21. D. Clover, B. Kinsella, B. Pejcic and R. De Marco, *Journal of Applied Electrochemestry*, 35 (2005) 139.
22. C.W. Du, X.G. Li, P. Liang, Z.Y. Liu, G.F. Jia and Y.F. Cheng, *Journal of Materials Engineering and Performance*, 18 (2009) 216.
23. J. Liu, Y. Lin, X. Yong, X. Li, *Corrosion*, 61 (2005) 1061.
24. U. Lotz, *Corrosion*/90, Paper no. 27 (Houston TX: NACE International, 1990).
25. D. Silverman, *Corrosion*/90, Paper no. 13 (Houston TX: NACE International, 1990).
26. Y.S. Choi, J.J. Shim, J.G. Kim, *ournal. of Alloys and Compunds*, 391 (2005) 162.
27. P.R. Rhodes, *Corros. Sci.,* 57 (2001) 923.
28. I. Hamada and K. Yamauchi, *Metall. Mater. Trans. A Phys. Metall. Mater. Sci.,* 5 (2010) 56.
29. CH. Ren, D. Liu, Z. Bai and T. Li, *Mater. Chem. Phys*., 93 (2005) 305.
30. D.W. Shoesmith, P. taylor, M.G. Bailey, D.G. Owen, *J. Electrochem. Soc.,* 127 (1980) 5.
31. A. Hernández-Espejel, M.A. Dominguez-Crespo, R. Cabrera-Sierra, C. Rodriguez-Meneses, E.M Arce-Estrada, *Corros. Sci*., 52 (2010) 2258.
32. S.A. Park, W.S. Ji, J.G. Kim, *Int. J. Electrochem. Sci*., 8 (2013) 7498.
33. D. Rickard and G. Luther, *Chem. Rev.*, 107 (2007) 514.
34. D. Rickard and J. Morse, *Mar. Chem*., 97 (2005) 141.
35. E. Díaz, J. Gonzalez-Rodriguez, R. Sandoval-Jabalera, S. Serna, B. Campillo, M. Neri_flores, C. Gaona-Tiburcio and A. Martínez-Villafane, *Int. J. Electrochem. Sci*., 5 (2010) 1821.
36. El-Sayed M. Sherif, Abdulhakim A. Almajid, Khalil Abdelrazek Khalil, Harri Junaedi and F.H. Latief, *Int. J. Electrochem. Sci*., 8 (2013) 9360.